Impaired brain glymphatic flow in experimental hepatic encephalopathy⋆

Anna Hadjihambi[1,2,†], **Ian F. Harrison**[3,†], **Marta Costas-Rodríguez**[4], **Frank Vanhaecke**[4], **Natalia Arias**[1], **Rocío Gallego-Durán**[5], **Svetlana Mastitskaya**[2], **Patrick S. Hosford**[2], **Steven W.M. Olde Damink**[6], **Nathan Davies**[1], **Abeba Habtesion**[1], **Mark F. Lythgoe**[3], **Alexander V. Gourine**[2], **Rajiv Jalan**[1,*]

[1]UCL Institute for Liver and Digestive Health, Division of Medicine, UCL Medical School, Royal Free Hospital, Rowland Hill Street, NW3 2PF London, UK

[2]Centre for Cardiovascular and Metabolic Neuroscience, Neuroscience, Physiology and Pharmacology, University College London, WC1E 6BT London, UK

[3]UCL Centre for Advanced Biomedical Imaging, Division of Medicine, University College London, WC1E 6BT London, UK

[4]Ghent University, Department of Chemistry, Atomic and Mass Spectrometry – A&MS Research Unit, Campus Sterre, Krijgslaan 281-S12, BE-9000 Ghent, Belgium

[5]Institute of Biomedicine of Sevilla (IBiS), Hospital Universitario Virgen del Rocío/CSIC/ Universidad de Sevilla, UCM Digestive Diseases & CIBERehd Sevilla, Spain

[6]Department of Surgery, Maastricht University, Maastricht, the Netherlands

Abstract

Background & Aims—Neuronal function is exquisitely sensitive to alterations in the extracellular environment. In patients with hepatic encephalopathy (HE), accumulation of metabolic waste products and noxious substances in the interstitial fluid of the brain is thought

to result from liver disease and may contribute to neuronal dysfunction and cognitive impairment. This study was designed to test the hypothesis that the accumulation of these substances, such as bile acids, may result from reduced clearance from the brain.

Methods—In a rat model of chronic liver disease with minimal HE (the bile duct ligation [BDL] model), we used emerging dynamic contrast-enhanced MRI and mass-spectroscopy techniques to assess the efficacy of the glymphatic system, which facilitates clearance of solutes from the brain. Immunofluorescence of aquaporin-4 (AQP4) and behavioural experiments were also performed.

Results—We identified discrete brain regions (olfactory bulb, prefrontal cortex and hippocampus) of altered glymphatic clearance in BDL rats, which aligned with cognitive/behavioural deficits. Reduced AQP4 expression was observed in the olfactory bulb and prefrontal cortex in HE, which could contribute to the pathophysiological mechanisms underlying the impairment in glymphatic function in BDL rats.

Conclusions—This study provides the first experimental evidence of impaired glymphatic flow in HE, potentially mediated by decreased AQP4 expression in the affected regions.

Lay summary—The 'glymphatic system' is a newly discovered brain-wide pathway that facilitates clearance of various substances that accumulate in the brain due to its activity. This study evaluated whether the function of this system is altered in a model of brain dysfunction that occurs in cirrhosis. For the first time, we identified that the clearance of substances from the brain in cirrhosis is reduced because this clearance system is defective. This study proposes a new mechanism of brain dysfunction in patients with cirrhosis and provides new targets for therapy.

Abstract
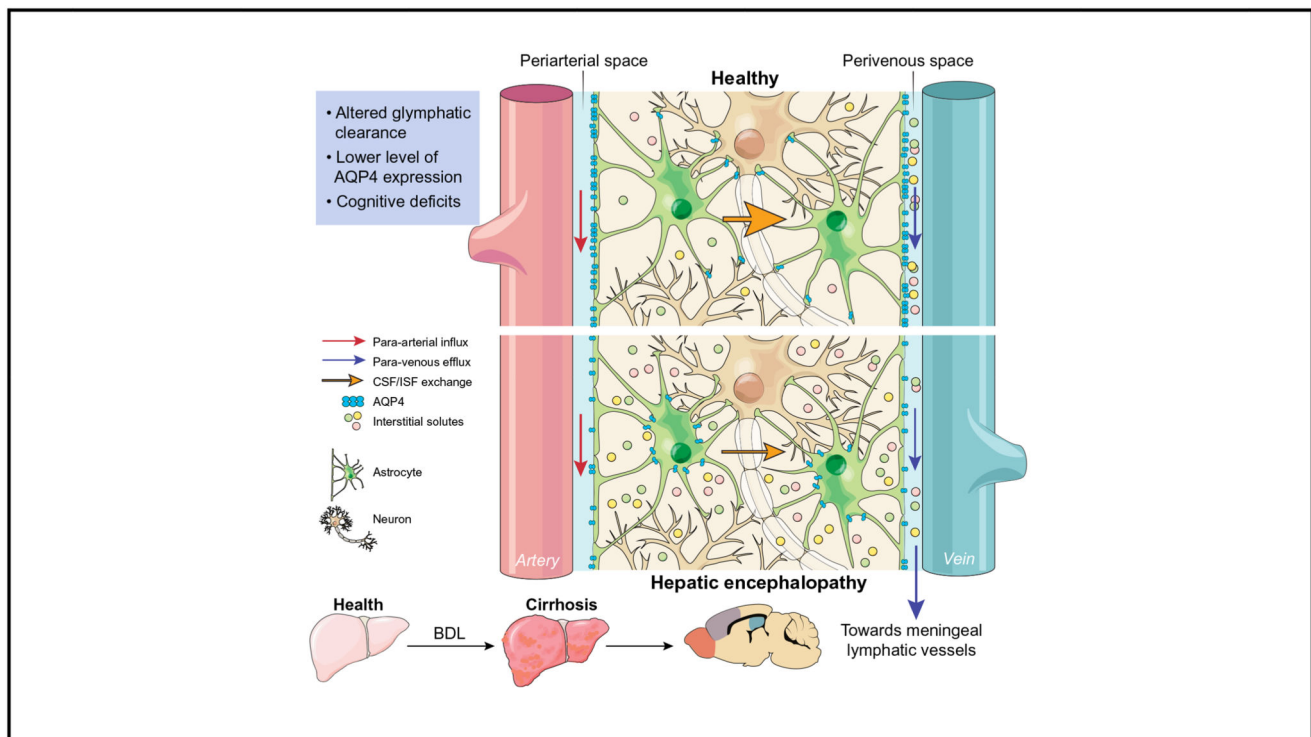
Graphic abstract.

Introduction

The mechanisms underlying the pathogenesis of hepatic encephalopathy (HE) in patients with cirrhosis (chronic liver disease) are not completely understood. Data available in the literature suggest that noxious substances and metabolites such as lactate, glutamate, bile acids and drugs accumulate in the brain of patients with HE.[1] The prevailing hypothesis proposes that this occurs because of metabolic and transporter defects induced by hyperammonaemia, inflammation and alterations in blood brain barrier function.[2,3]

In the periphery, the lymphatic system is responsible for interstitial fluid (ISF) clearance, a mechanism that is critical for maintaining tissue homeostasis. Although neuronal function is exquisitely sensitive to alterations in the extracellular environment, until recently, the brain was believed to be devoid of a lymphatic drainage/clearance system. Recent studies identified a brain-wide paravascular pathway that facilitates the efficient clearance of various molecules, including toxic interstitial proteins, lactate and other metabolites.[4,5] Subarachnoid cerebrospinal fluid (CSF) circulates through the brain parenchyma along the paravascular spaces surrounding penetrating arteries, exchanging with the surrounding ISF and facilitating the clearance of interstitial solutes.[4] ISF is then cleared along paravascular spaces surrounding large calibre cerebral veins, which reach the recently discovered meningeal lymphatic vessels[6] and enter the systemic circulation. This pathway has been termed the "glymphatic system" because of its apparent dependence on glial water channels and its clearance function similar to that of the lymphatic system. That said, the precise definition of what constitutes "glymphatic" function in the brain is still being debated and discussed in the literature,[7–9] and the precise role that glial water channels play in such a clearance pathway is unclear. A schematic describing this system in health and HE (according to the findings of the current study) is depicted in Fig. 1.

In addition to clearing the brain, the glymphatic system is thought to contribute to the distribution of growth factors, neuromodulators, carrier proteins and other solutes within the brain.[10] Failure of the glymphatic system (achieved either experimentally[11] or pathophysiologically[12–15]) may therefore have critical adverse consequences, and has been linked to the pathogenesis of neurodegenerative disease(s).[5,16]

In this study, we tested the hypothesis that the glymphatic clearance mechanisms are impaired in cirrhosis, potentially contributing to the development of the neurochemical phenotype observed in HE. Making use of the bile duct ligation (BDL) rat model of chronic liver disease with minimal HE, we used mass-spectroscopy techniques as well as cisternal delivery of an MRI contrast agent, and dynamic contrast-enhanced MRI (used previously to define the function of the glymphatic system in rodents[4,13,17–21] and in humans[22–26]) to measure the relative function of this system in the diseased (HE) and healthy rat brain.

Materials and methods

Animal models

All the experiments were performed in accordance with the Animals (Scientific Procedures) Act 1986 (ASPA) revised according to the European Directive 2010/63/EU and the UK Home Office (Scientific Procedures) Act (1986) with prior project approval from UCL's internal Animal Welfare and Ethical Review Body. Male Sprague-Dawley rats (body weight ~350–400 g) were obtained from a commercial supplier (Charles Rivers Laboratories, Inc., Oxford), and transported to UCL at least 14 days prior to experimentation. Rats were group housed (3 per cage) in individually ventilated cages kept on a 12 h light-dark cycle (light 7 am-7 pm), with *ad libitum* access to standard rat chow and water, and environment enrichment in the form of chew sticks and cardboard tubes.

A total of 46 animals were used in this project in the different sub-studies. BDL and sham surgeries were performed as previously reported[27] on 22 and 24 animals respectively (Details on surgical protocol in the supplementary section).

Blood and brain tissue were collected under terminal isoflurane anaesthesia. Plasma biochemistry was performed using a Cobas Integra II system (Roche Diagnostics).

Dynamic contrast-enhanced MRI

Five sham-operated and 5 BDL rats were anaesthetised, the dura mater overlaying the cisterna magna was exposed and an intrathecal 24-gauge infusion catheter (0.7×19 mm, B|Braun, Melsungen, Germany) was advanced 1 mm into the cisternal space. Following surgery, animals were transferred to an MRI compatible cradle with a snout mask positioned to deliver 1.5% isoflurane in oxygen. Rats were maintained at 37 °C core body temperature and respiratory rate was maintained between 70 and 100 breaths per minute. All imaging was performed with a 9.4 T VNMRS horizontal bore MR scanner (Agilent Inc., Santa Clara, California, USA). A baseline scan was acquired prior to intrathecal infusion of the paramagnetic contrast agent, gadolinium (Gd-DTPA, 21 mM) via the pre-implanted catheter (80 μl at 1.6 μl/min, total time 50 min). MR images were continually acquired throughout and after intrathecal infusion for a total time of 144 min. At the end of the experiment the animal was euthanised by sodium pentobarbital overdose (200 mg/kg). Details on surgical protocol, image acquisition and processing are available in the supplementary section.

Intracranial pressure measurements

In a separate group of BDL (n = 6) and sham-operated (n = 8) animals, resting intracranial pressure (ICP) was determined. Under general anaesthesia (5% isoflurane in oxygen for induction, 2% isoflurane in air for maintenance), the femoral artery was cannulated for blood pressure measurements. The rats were positioned in a stereotaxic frame with the head flexed to 50° and a midline incision was made at a midpoint between the skull base and the occipital margin to the first vertebrae. The underlying muscles were parted exposing the atlanto-occipital membrane and dura mater overlaying the cisterna magna. A 23-gauge needle attached to a cannula connected to a pressure transducer was inserted into the cisterna magna and the system was sealed immediately using surgical glue. The animal was allowed

to recover for 15 min and the ICP was recorded. Data from previous studies have shown no significant alterations in ICP during the chosen volume and rate of cisterna magna contrast agent infusion.[28]

Microinjections of Gd-DTPA in the prefrontal cortex evaluating brain tissue clearance

Under general anaesthesia (5% isoflurane in oxygen for induction, 2% isoflurane in air for maintenance) another 6 BDL and 6 sham-operated rats underwent a stereotaxic micro-infusion of 4 μl Gd-DTPA (Magnevist® 860 mM Gd-DTPA, MW 938 Da; Schering Health Care Ltd. in water for injection) into the left prefrontal cortex (anteroposterior, +2 mm, mediolateral, +3 mm and dorsal to ventral, –1.75 mm, relative to bregma) using a 10 μl glass Hamilton syringe (4 μl at 0.4 μl/min, total time 10 min). After 30 min of the intracerebral infusion, the cisterna magna was exposed and was thoroughly cleaned with saline. A durotomy was made using a 23-gauge needle attached to a 1 ml syringe, allowing CSF to be collected. At the end of the experiment the animals were euthanised by overdose of sodium pentobarbital (200 mg/kg, i.p). Blood was collected from the left ventricle of the heart. The brain was also quickly removed from the skull and dissected into the frontal (~–2.5 mm from bregma forward), middle (~–2.5 to –10 mm from bregma), and the hind brain (~–10 mm from bregma backwards). All samples (blood plasma, CSF, brain tissue) were snap frozen in liquid nitrogen and Gd-DTPA, as well as total tauro-conjugated bile acids (in plasma and CSF), quantification was performed using sector-field ICP-mass spectrometry (SF-ICP-MS) (details are available in the supplementary section).

AQP4 immunofluorescence and blood vessel labelling

Four BDL and 4 sham-operated animals were terminally anesthetised with urethane (1.9 g/kg i.p.) and transcardially perfused with ice-cold 0.9% sodium chloride solution followed by 4% paraformaldehyde (PFA) at 4 °C. Brains were removed, post-fixed in PFA overnight, and cryoprotected in 30% sucrose for 48 h at 4 °C. Coronal brain slices (30 μm) were sectioned using a cryostat (Bright instruments, UK).

Olfactory bulb and prefrontal cortex sections were incubated in blocking buffer for 2 h on a shaker, to minimise non-specific binding of the antibody (10% goat serum in 0.1% Triton in PBS). Tissue was then incubated in primary antibody aquaporin-4 (AQP4, 1:60, ab9512, Mouse monoclonal, Abcam) diluted in blocking buffer for 24 h at 4 °C on a shaker. Negative controls were performed for each animal group by omitting the primary antibody in one of the wells. Tissue was washed 3 times with PBS for 10 min and subsequently incubated in the secondary antibody, Alexa 568 anti-mouse (1:500, Molecular probes) together with Alexa Fluor™ 647 Conjugate Isolectin B_4 (1:200, Molecular Probes: I32450), diluted in the blocking buffer, for 24 h at 4 °C on a shaker. Isolectin B_4 binds to α-D-galactose residues in the basement membrane secreted by endothelial cells.[29] After 3 final washes in PBS, the tissue was mounted on glass slides and cover-slipped with Fluoroshields (Sigma). Slides were then imaged using a Zeiss LSM 700 confocal microscope.

Quantification of AQP4 expression

Evaluation of the localisation of AQP4 to perivascular end-feet and glial limitans was performed by measuring the pixel intensities of Isolectin and AQP4 immunoreactivity across

cross sections of blood vessels in each brain region studied. For this, fluorescent intensity for both Isolectin and AQP4 markers were measured across a single 40 μm axis perpendicular to the vessel orientation, and expressed as intensity, normalised to the intensity of a randomly selected background region of interest (ROI) in the same image for each antigen, to generate linear plots of fluorescence extending from the brain tissue, into the vessel and again into the surrounding brain tissue.

Quantification of AQP4 polarisation

Perivascular polarisation of AQP4 was measured as previously described.[10] Briefly, the median immunofluorescence intensity of AQP4 immunopositivity in perivascular regions was measured. A threshold analysis was then used to measure the percentage of the region exhibiting AQP4 immunofluorescence greater than or equal to perivascular AQP4 immunofluorescence (AQP4% area). Polarisation was expressed as the percentage of the region that exhibited lower AQP4 immunoreactivity than the perivascular end-feet. AQP4 vessel coverage was measured by firstly delineating the area of the vessel from the Isolectin channel image. This ROI was then placed on the AQP4 channel image thresholded for immunoreactivity, for extraction of the percentage vessel coverage (% immunoreactivity of AQP4 of whole delineated vessel).

Behavioural experiments

Spatial working memory, evaluating prefrontal cortex function, in separate groups of sham-operated (n = 5) and BDL rats (n = 5) was evaluated in the Barnes Maze. The training consisted of 1 day for habituation followed by the working memory training which involved a paired sample task during the following 6 days of training. Each daily session consisted of 2 identical trials (sample and retention). During both trials, the escape box was in a fixed position every day, changing between days in a pseudorandom order (details are available in the supplementary section).

To test the reference memory in the Barnes Maze and evaluate hippocampal function, the escape box remained in the same position during the training session for 5 days. Visual cues were placed above the 4 quadrants of the maze and 4 trials were performed per day for 5 days. Time spent to find the target hole where the escape box used to be located (latency), distance travelled, speed and path efficiency (1 indicates perfect efficiency-animal moved in a straight line) were recorded and analysed by ANY-maze software (Stoelting Co) (details are available in the supplementary section).

Statistical analysis

Statistical comparisons between MR time course data and the brain SF-ICP-MS data from sham-operated and BDL groups were performed using 2-way ANOVA followed by Bonferroni *post hoc* test. CSF and plasma SF-ICP-MS as well as ICP data from sham-operated and BDL groups were compared using a Student's *t* test. Biochemistry data was analysed using one-way ANOVA.

Statistical comparisons between immunofluorescence line profile data, area under the curve from line profile data and AQP4 vessel coverage and polarisation from sham-operated and BDL groups were performed using 2-way ANOVA followed by Bonferroni *post hoc* test.

For the neurobehavioural experiments, statistical comparisons of data between sham-operated and BDL animals were performed using 2-way ANOVA with Bonferroni *post hoc* test. For comparison of data within animal groups along training days, 2-way ANOVA was applied followed by Tukey *post hoc* test.

Statistical tests were performed using GraphPad Prism (v6 for Windows, San Diego, CA, USA), and all data were reported as mean ± SEM. Differences with *p* value of <0.05 were considered significant. Sample sizes were calculated using Gpower 3 v3.1.9.2 (http://www.gpower.hhu.de/en.html)[30] using a 'means: ANOVA (two groups)' test, with a desired power of 90% and a significance level of 5%. The effect size was calculated from the difference in contrast infiltration observed in the olfactory bulb of sham and BDL animals in a preliminary study (n = 3). Based on this calculation, n = 5 was used. The same calculations were performed for the other experiments when possible, in order to determine appropriate n numbers.

For further details regarding the materials and methods used, please refer to the CTAT table and supplementary information.

Results

Biochemistry

Plasma biochemistry, including ammonia concentration, was assessed in all groups of animals (Table S1). Compared to sham surgery, BDL resulted in a significant increase in plasma alanine aminotransferase and bilirubin (*p* <0.001), indicating impaired liver function, while albumin and total protein concentrations were significantly decreased (*p* <0.001). Plasma ammonia concentration was significantly higher in BDL rats compared to sham-operated animals (*p* <0.001). The level of total tauro-conjugated bile acids was also significantly higher in both the plasma and CSF (*p* <0.001) in BDL compared to sham animals (Table S1).

Glymphatic flow evaluated using dynamic contrast-enhanced MRI

Dynamic contrast-enhanced MRI was used to visualise brain-wide subarachnoid CSF-ISF exchange in anesthetised BDL and sham-operated animals. The time course of parenchymal distribution of the paramagnetic contrast agent, Gd-DTPA throughout the brain was assessed as a measure of glymphatic flow.[4,5] Following an intra-cisternal infusion of gadolinium, serial acquisition of T1-weighted MR images was performed (Fig. 2A). The integrity of the skull was confirmed by monitoring the temporalis muscle for the presence of gadolinium (Fig. 3E), to ensure a sealed and intact system, which is essential for the glymphatic flow.

In order to assess the ability of the brain to distribute the infused contrast agent, the brain was compartmentalised (on analysis) and the quantification of signal intensity vs. time of inflow was compared between BDL and sham-operated animals. Parenchymal penetration

of the contrast agent in the olfactory bulb ($p < 0.0001$) and prefrontal cortex ($p = 0.01$) was dramatically reduced in BDL rats compared to sham-operated animals, indicating that the efficacy of glymphatic flow in these areas is compromised (Fig. 2C-D). In contrast, facilitated inflow of contrast agent was observed in the hippocampus ($p = 0.03$) of BDL rats (Fig. 2E), further suggesting that glymphatic flow is altered in this HE model.

CSF filled compartments, including the aqueduct, third and lateral ventricles, showed no significant differences in inflow between sham-operated and BDL animals (Fig. 4A-D). Similarly, time courses of the parenchymal distribution of the contrast agent in the striatum ($p = 0.4$), midbrain ($p = 0.7$), caudal cortex ($p = 0.1$), thalamus ($p = 0.06$) and hypothalamus ($p = 0.2$) were not different between the two groups (Fig. 3A-D, F).

Glymphatic clearance evaluated via Gd-DTPA quantification using SF-ICP-MS

Following the assessment of glymphatic flow by MRI, a separate cohort of animals was intracerebrally infused with Gd-DTPA, the same imaging agent used for the MRI experiments. The aim of these experiments evaluating the clearance of Gd-DTPA from the brain was to validate the results of impaired glymphatic inflow that were observed using MRI.

Thirty minutes after the Gd-DTPA was infused in the pre-frontal cortex, one of the most altered and accessible brain regions according to the MRI results, blood plasma and CSF were collected. Additionally, the brain was removed and dissected into frontal (site of infusion), middle and hind brain regions. The Gd-DTPA concentration in samples was then quantified using SF-ICP-MS, revealing a trend towards less Gd-DTPA in circulating plasma ($p = 0.5$) and CSF ($p = 0.2$) of BDL rats, however these differences were not significant. These data suggest that less Gd-DTPA had been cleared out of the brain of BDL animals (Fig. 5A-B). In line with these data, significantly higher Gd-DTPA content was recorded in the frontal brain tissue of BDL compared to sham-operated rats ($p < 0.001$), while the other regions did not show significant differences in Gd-DTPA content (Fig. 5C). This suggests that Gd-DTPA clearance from the pre-frontal cortex is also impaired in BDL rats, similar to glymphatic inflow in this region.

Measurement of intracranial pressure and volume of the brain regions of interest in sham-operated and BDL animals

Impairment of parenchymal contrast agent penetration and clearance could be due to altered ICP, or brain volume differences in BDL animals. Therefore, volumes of select brain regions, obtained from 3D ROI measurements of contrast-enhanced MR images (Fig. 4D) and recorded ICP from the cisterna magna (Fig. 2B), were then determined in sham-operated (n = 8) and BDL (n = 6) animals. The results obtained demonstrated that the observed contrast agent inflow and impaired clearance cannot be attributed to altered pressure or volume differences in the brain, as the volumes of brain regions ($p > 0.05$ for all regions) and the ICP recorded from the cisterna magna ($p = 0.7$) were not different between sham-operated and BDL animals.

Evaluation of AQP4 expression and polarisation in the brain regions of interest in sham-operated and BDL animals

The astrocytic water channel AQP4, which is highly polarised on astrocytic end-feet, ensheathing brain vasculature, has been shown to play an important role in the transport of CSF into the brain parenchyma via the glymphatic system.[5] It has also been shown that with advancing age, glymphatic function is reduced, possibly caused by astrocytic activation, associated with altered AQP4 expression and localisation.[10] In order to better understand the underlying mechanism of impaired glymphatic function observed in animal models of HE, we performed AQP4 immunofluorescence analysis and blood vessel labelling with Isolectin in the two most affected brain regions; the olfactory bulb and prefrontal cortex.

On the dual fluorescence images obtained, lines were drawn across blood vessels and intensity measurements were made for both AQP4 and Isolectin across vessel cross sections (Fig. S1). Analysing the expression of AQP4 and Isolectin we observed that, in the olfactory bulb, Isolectin and AQP4 intensities appeared similar between vessels from sham-operated and BDL rats (Fig. 6A-B). While in the prefrontal cortex, Isolectin appeared more intense in BDL rats, with a difference between AQP4 intensities between groups (Fig. 6C-D). To simplify the intensity measurements, we analysed the area under the curve of the peaks and observed significantly lower AQP4 expression compared to Isolectin in both the olfactory bulb ($p < 0.05$) and prefrontal cortex ($p < 0.01$) of BDL rats, which was not the case in sham-operated animals (Fig. 6E).

Furthermore, both AQP4 polarisation (degree to which AQP4 expression is polarised to blood vessels) and AQP4 vessel coverage (average% area of selected blood vessel which is covered by AQP4) were measured. AQP4 polarisation (Fig. 7A, olfactory bulb: $p = 0.3$; prefrontal cortex: $p = 0.4$) as well as vessel coverage (Fig. 7B, olfactory bulb: $p = 0.1$; prefrontal cortex: $p = 0.1$) showed a trend towards lower vessel AQP4 expression in BDL compared to sham-operated rats, though none of these changes were statistically significant.

Evaluation of prefrontal cortex function: Spatial working memory

To determine the possible functional consequences of altered glymphatic flow and clearance, an array of behavioural and cognitive tests was performed in BDL (n = 5) and sham-operated (n = 5) animals. The prefrontal cortex is critically involved in cognitive functions such as working memory, a process of maintaining an active representation of information available for use, as well as organisation and planning of responses.[31] Testing spatial working memory in the Barnes Maze was then used to assess the function of prefrontal cortex. While there was no difference between the animal groups in time required to reach the escape box during the sample trial ($p = 0.3$) (training on the day to learn the new location of the escape box), significant differences between the BDL and sham-operated animals in the retention trial ($p = 0.02$) were recorded (Fig. 8A-B). These data suggest that the BDL animals are unable to retain an active representation of information, indicating impaired prefrontal cortex function.

Evaluation of hippocampal function: Spatial reference memory

As the hippocampus is important in the acquisition of spatial reference memory[32], further tests to assess its function were performed in the Barnes Maze. Although no differences were observed in escape latencies between BDL and sham-operated animals ($p = 0.2$), the control group showed a progressive and significant improvement in the task acquisition during the training days ($p = 0.01$), which was not observed in the BDL animals ($p > 0.05$) (Fig. 8C). This indicates the inability of BDL animals to learn how to use the reference cues in order to reach the escape box, suggesting potential impairment of hippocampal function. There were no differences in the speed ($p = 0.4$) and distance travelled ($p = 0.4$) between the two groups of animals, suggesting that the observed differences in latency were not due to the potential locomotor deficiency in the BDL rats (Fig. 8D-E). Moreover, the learning ability of sham-operated, but not of BDL animals, was observed through the significant decrease in distance covered (within the group, $p < 0.001$), which was also reflected in the increase of path efficiency ($p = 0.01$) along training days (Fig. 8F). These results demonstrate a functional modification to the observed alteration in glymphatic flow in the hippocampus.

Discussion

Many diseases, mainly neurodegenerative, are associated with accumulation of cellular waste products such as by-products of metabolism and cellular respiration. Intracellular proteasomal degradation and autophagy are considered the principal means of removing proteins from the central nervous system and the dysfunction of these processes has been associated with neurodegeneration.[33] Yet, many cytosolic proteins are released into the interstitial space of the brain, suggesting that effective disposal routes should exist to eliminate such waste. Data exist showing the accumulation of many noxious substances and metabolites in the ISF and CSF collected from the brain of patients with HE,[1] but the underlying mechanisms are not clear. The data described herein, demonstrating an impairment of the glymphatic system in BDL animals (Fig. 1), suggest that a lack of clearance may contribute to the accumulation of noxious substances in the brains of patients with cirrhosis.

Using two lines of evidence; MRI and SF-ICP-MS, this study demonstrates, for the first time, impaired CSF penetration and parenchymal clearance of the contrast agent in frontal brain regions (the olfactory bulb and prefrontal cortex) of BDL rats, indicating a clear dysfunction of the glymphatic clearance system in an animal model of chronic liver disease and HE. The reasons underlying increased contrast agent inflow in the hippocampus are currently unclear, but may be due to cell loss/neurodegeneration, also seen in animal models of Alzheimer's disease or regional glial alterations that may occur in HE.[34] Cytotoxic oedema and energy depletion, which are known features of HE, enhance glymphatic CSF influx while suppressing ISF efflux,[35] which may also contribute to the increased contrast inflow in the hippocampus. The data showing memory deficits in this model of HE provide evidence of functional modifications, indicating impaired prefrontal cortex function as well as potential derangement in hippocampal-prefrontal cortex connections.

The pathophysiological mechanisms underlying impaired glymphatic flow reported here are unclear. While we have excluded the possibility of increased ICP and brain volume contributing to this phenotype, our data suggest that significantly lower AQP4 expression compared to the vasculature marker in both the olfactory bulb and prefrontal cortex of BDL rats, could contribute to the pathophysiological mechanisms underlying the impaired glymphatic function. Furthermore, the moderately altered AQP4 vessel coverage as well as polarisation could also eventually contribute to altering glymphatic flow. This is an important observation as other studies have proposed that changes in AQP4 expression, localisation, or function may alter glymphatic pathway function and contribute to the development of Alzheimer's disease or other neurodegenerative conditions in animal models[10] and in humans.[22] Several other factors, some known to be deranged in HE, such as reactive astrogliosis,[36] hemichannel dysfunction,[3] altered neuronal activity,[35] arterial pulse-pressure,[37] and central nervous system inflammation,[38] may also play a role. Interestingly, many of these factors are prominent in other diseases[10] and could represent important therapeutic targets to restore paravascular CSF-ISF exchange.

Maintenance of volume homeostasis of cells requires energy. Energy depletion can cause brain cell swelling termed cytotoxic oedema.[39] From extensive studies on HE rodent models, it is known that ammonia plays a direct role in the development of this astrocytic oedema,[40] although this is mild in cirrhosis and associated HE. Astrocytic end-feet interpose a high-resistance barrier to fluid-solute flux between paravascular and interstitial compartments. Pericyte and microglial processes are also scattered in between the vascular wall and astrocyte end-feet, which creates a filter size of glial barrier large enough for nearly all-mammalian proteins (~35 kDa and diameter 2–3 nm, including serum albumin ~70 kDa and 4–6 nm diameter). Astrocytic swelling (extending to end-feet) can therefore interfere with the clearance of the brain by obstructing the paravascular CSF-ISF exchange and solute clearance.

An interesting idea proposed by Thrane et al.,[35] suggests that gap-junction connections between astrocytes might rapidly distribute Na^+-influx across the glial syncytium.[41,42] Na^+ and Cl^- redistribution would in turn make ISF slightly hypo-osmolar relative to CSF,[43] which would build an osmotic ISF-CSF gradient that in theory would pull CSF into the ISF compartment. A study from our group already demonstrated functional hemichannel dysfunction in the cerebral cortex of BDL animals.[3] This dysfunction could also extend to the gap-junction level, preventing the distribution of these ions and therefore the development of an osmotic gradient, which will consequently diminish the efficacy of the glymphatic clearance pathway as demonstrated here. This hypothesis will need to be tested in future studies.

In conclusion, this study provides the first experimental evidence of impaired glymphatic inflow and clearance in a rodent model of chronic liver disease and HE, with decreased expression of AQP4 suggested to play a mechanistic role.

Supplementary Material

Refer to Web version on PubMed Central for supplementary material.

Financial support

References

Author names in bold designate shared co-first authorship

[1]. Weiss N, Barbier Saint Hilaire P, Colsch B, Isnard F, Attala S, Schaefer A, et al. Cerebrospinal fluid metabolomics highlights dysregulation of energy metabolism in overt hepatic encephalopathy. J Hepatol. 2016; 65: 1120–1130. DOI: 10.1016/j.jhep.2016.07.046 [PubMed: 27520878]

[2]. Shawcross DL, Shabbir SS, Taylor NJ, Hughes RD. Ammonia and the neutrophil in the pathogenesis of hepatic encephalopathy in cirrhosis. Hepatology. 2010; 51 (3) 1062–1069. DOI: 10.1002/hep.23367 [PubMed: 19890967]

[3]. Hadjihambi A, De Chiara F, Hosford PS, Habtetion A, Karagiannis A, Davies N, et al. Ammonia mediates cortical hemichannel dysfunction in rodent models of chronic liver disease. Hepatology. 2017; 65 (4) 1306–1318. DOI: 10.1002/hep.29031 [PubMed: 28066916]

[4]. Iliff JJ, Lee H, Yu M, Feng T, Logan J, Nedergaard M, et al. Brain-wide pathway for waste clearance captured by contrast-enhanced MRI. J Clin Invest. 2013; 123 (3) 1299–1309. DOI: 10.1172/JCI67677 [PubMed: 23434588]

[5]. Iliff JJ, Wang M, Liao Y, Plogg BA, Peng W, Gundersen GA, et al. A paravascular pathway facilitates CSF flow through the brain parenchyma and the clearance of interstitial solutes, including amyloid beta. Sci Transl Med. 2012; 4 (147) 147ra11 doi: 10.1126/scitranslmed.3003748

[6]. Louveau A, Smirnov I, Keyes TJ, Eccles JD, Rouhani SJ, Peske JD, et al. Structural and functional features of central nervous system lymphatic vessels. Nature. 2015; 523 (7560) 337–341. DOI: 10.1038/nature14432 [PubMed: 26030524]

[7]. Bacyinski A, Xu M, Wang W, Hu J. The paravascular pathway for brain waste clearance: current understanding, significance and controversy. Front Neuroanat. 2017; 11 101 doi: 10.3389/fnana.2017.00101 [PubMed: 29163074]

[8]. Nakada T, Kwee IL. Fluid dynamics inside the brain barrier: current concept of interstitial flow, glymphatic flow, and cerebrospinal fluid circulation in the brain. Neuroscientist. 2018; 1073858418775027 doi: 10.1177/1073858418775027

[9]. Abbott NJ, Pizzo ME, Preston JE, Janigro D, Thorne RG. The role of brain barriers in fluid movement in the CNS: is there a 'glymphatic' system? Acta Neuropathol. 2018; 135 (3) 387–407. DOI: 10.1007/s00401-018-1812-4 [PubMed: 29428972]

[10]. Kress BT, Iliff JJ, Xia M, Wang M, Wei HS, Zeppenfeld D, et al. Impairment of paravascular clearance pathways in the aging brain. Ann Neurol. 2014; 76 (6) 845–861. DOI: 10.1002/ana.24271 [PubMed: 25204284]

[11]. Lundgaard I, Lu ML, Yang E, Peng W, Mestre H, Hitomi E, et al. Glymphatic clearance controls state-dependent changes in brain lactate concentration. J Cereb Blood Flow Metab. 2017; 37 (6) 2112–2124. DOI: 10.1177/0271678X16661202 [PubMed: 27481936]

[12]. Achariyar TM, Li B, Peng W, Verghese PB, Shi Y, McConnell E, et al. Glymphatic distribution of CSF-derived apoE into brain is isoform specific and suppressed during sleep deprivation. Mol Neurodegener. 2016; 11 (1) 74 doi: 10.1186/s13024-016-0138-8 [PubMed: 27931262]

[13]. Jiang Q, Zhang L, Ding G, Davoodi-Bojd E, Li Q, Li L, et al. Impairment of the glymphatic system after diabetes. J Cereb Blood Flow Metab. 2017; 37 (4) 1326–1337. DOI: 10.1177/0271678X16654702 [PubMed: 27306755]

[14]. Plog BA, Nedergaard M. The glymphatic system in central nervous system health and disease: past, present, and future. Annu Rev Pathol. 2018; 13: 379–394. DOI: 10.1146/annurev-pathol-051217-111018 [PubMed: 29195051]

[15]. Sullan MJ, Asken BM, Jaffee MS, DeKosky ST, Bauer RM. Glymphatic system disruption as a mediator of brain trauma and chronic traumatic encephalopathy. Neurosci Biobehav Rev. 2018; 84: 316–324. DOI: 10.1016/j.neubiorev.2017.08.016 [PubMed: 28859995]

[16]. Peng WG, Achariyar TM, Li BM, Liao YH, Mestre H, Hitomi E, et al. Suppression of glymphatic fluid transport in a mouse model of Alzheimer's disease. Neurobiol Dis. 2016; 93: 215–225. DOI: 10.1016/j.nbd.2016.05.015 [PubMed: 27234656]

[17]. Benveniste H, Lee H, Ding F, Sun Q, Al-Bizri E, Makaryus R, et al. Anesthesia with dexmedetomidine and low-dose isoflurane increases solute transport via the glymphatic pathway in rat brain when compared with high-dose isoflurane. Anesthesiology. 2017; 127 (6) 976–988. DOI: 10.1097/ALN.0000000000001888 [PubMed: 28938276]

[18]. Gaberel T, Gakuba C, Goulay R, Martinez De Lizarrondo S, Hanouz JL, Emery E, et al. Impaired glymphatic perfusion after strokes revealed by contrast-enhanced MRI: a new target for fibrinolysis? Stroke. 2014; 45 (10) 3092–3096. DOI: 10.1161/STROKEAHA.114.006617 [PubMed: 25190438]

[19]. Gakuba C, Gaberel T, Goursaud S, Bourges J, Di Palma C, Quenault A, et al. General anesthesia inhibits the activity of the "glymphatic system". Theranostics. 2018; 8 (3) 710–722. DOI: 10.7150/thno.19154 [PubMed: 29344300]

[20]. Lee H, Mortensen K, Sanggaard S, Koch P, Brunner H, Quistorff B, et al. Quantitative Gd-DOTA uptake from cerebrospinal fluid into rat brain using 3D VFA-SPGR at 9.4T. Magn Reson Med. 2018; 79 (3) 1568–1578. DOI: 10.1002/mrm.26779 [PubMed: 28627037]

[21]. Lee H, Xie L, Yu M, Kang H, Feng T, Deane R, et al. The effect of body posture on brain glymphatic transport. J Neurosci. 2015; 35 (31) 11034–11044. DOI: 10.1523/JNEUROSCI.1625-15.2015 [PubMed: 26245965]

[22]. Eide PK, Ringstad G. MRI with intrathecal MRI gadolinium contrast medium administration: a possible method to assess glymphatic function in human brain. Acta Radiol Open. 2015; 4 (11) doi: 10.1177/2058460115609635 2058460115609635 [PubMed: 26634147]

[23]. Eide PK, Ringstad G. Delayed clearance of cerebrospinal fluid tracer from entorhinal cortex in idiopathic normal pressure hydrocephalus: a glymphatic magnetic resonance imaging study. J Cereb Blood Flow Metab. 2018; doi: 10.1177/0271678X18760974 271678X18760974

[24]. Eide PK, Vatnehol SAS, Emblem KE, Ringstad G. Magnetic resonance imaging provides evidence of glymphatic drainage from human brain to cervical lymph nodes. Sci Rep. 2018; 8 (1) 7194 doi: 10.1038/s41598-018-25666-4 [PubMed: 29740121]

[25]. Ringstad G, Valnes LM, Dale AM, Pripp AH, Vatnehol SS, Emblem KE, et al. Brain-wide glymphatic enhancement and clearance in humans assessed with MRI. JCI Insight. 2018; 3 (13) doi: 10.1172/jci.in-sight.121537

[26]. Ringstad G, Vatnehol SAS, Eide PK. Glymphatic MRI in idiopathic normal pressure hydrocephalus. Brain. 2017; 140 (10) 2691–2705. DOI: 10.1093/brain/awx191 [PubMed: 28969373]

[27]. Harry D, Anand R, Holt S, Davies S, Marley R, Fernando B, et al. Increased sensitivity to endotoxemia in the bile duct-ligated cirrhotic Rat. Hepatology. 1999; 30 (5) 1198–1205. DOI: 10.1002/hep.510300515 [PubMed: 10534341]

[28]. Yang L, Kress BT, Weber HJ, Thiyagarajan M, Wang B, Deane R, et al. Evaluating glymphatic pathway function utilizing clinically relevant intrathecal infusion of CSF tracer. Journal of Translational Medicine. 2013; 11 107 doi: 10.1186/1479-5876-11-107 [PubMed: 23635358]

[29]. Peters BP, Goldstein IJ. The use of fluorescein-conjugated Bandeiraea simplicifolia B4-isolectin as a histochemical reagent for the detection of alpha-D-galactopyranosyl groups. Their occurrence in basement membranes. Exp Cell Res. 1979; 120: 321–334. [PubMed: 436961]

[30]. Faul F, Erdfelder E, Buchner A, Lang AG. Statistical power analyses using G*Power 3.1: tests for correlation and regression analyses. Behav Res Methods. 2009; 41 (4) 1149–1160. DOI: 10.3758/BRM.41.4.1149 [PubMed: 19897823]

[31]. Fuster JM. Behavioral electrophysiology of the prefrontal cortex of the primate. Progr Brain Res. 1990; 85: 313–323.

[32]. Li L, Sase A, Patil S, Sunyer B, Hoger H, Smalla KH, et al. Distinct set of kinases induced after retrieval of spatial memory discriminate memory modulation processes in the mouse hippocampus. Hippocampus. 2013; 23 (8) 672–683. DOI: 10.1002/hipo.22127 [PubMed: 23536525]

[33]. Nedelsky NB, Todd PK, Taylor JP. Autophagy and the ubiquitin-protea-some system: collaborators in neuroprotection. Biochim Biophys Acta. 2008; 1782 (12) 691–699. DOI: 10.1016/j.bbadis.2008.10.002 [PubMed: 18930136]

[34]. Hernandez-Rabaza V, Cabrera-Pastor A, Taoro-Gonzalez L, Malaguarnera M, Agusti A, Llansola M, et al. Hyperammonemia induces glial activation, neuroinflammation and alters neurotransmitter receptors in hippocampus, impairing spatial learning: reversal by sulforaphane. J Neuroin-flamm. 2016; 13 41 doi: 10.1186/s12974-016-0505-y

[35]. Thrane AS, Rangroo Thrane V, Nedergaard M. Drowning stars: reassessing the role of astrocytes in brain edema. Trends Neurosci. 2014; 37 (11) 620–628. DOI: 10.1016/j.tins.2014.08.010 [PubMed: 25236348]

[36]. Iliff JJ, Chen MJ, Plog BA, Zeppenfeld DM, Soltero M, Yang L, et al. Impairment of glymphatic pathway function promotes tau pathology after traumatic brain injury. J Neurosci. 2014; 34 (49) 16180–16193. DOI: 10.1523/INEUROSCI.3020-14.2014 [PubMed: 25471560]

[37]. Iliff JJ, Wang M, Zeppenfeld DM, Venkataraman A, Plog BA, Liao Y, et al. Cerebral arterial pulsation drives paravascular CSF-interstitial fluid exchange in the murine brain. J Neurosci. 2013; 33 (46) 18190–18199. DOI: 10.1523/JNEUROSCI.1592-13.2013 [PubMed: 24227727]

[38]. Erickson MA, Hartvigson PE, Morofuji Y, Owen JB, Butterfield DA, Banks WA. Lipopolysaccharide impairs amyloid beta efflux from brain: altered vascular sequestration, cerebrospinal fluid reabsorption, peripheral clearance and transporter function at the blood-brain barrier. J Neuroinflamm. 2012; 9 150 doi: 10.1186/1742-2094-9-150

[39]. Thrane AS, Rappold PM, Fujita T, Torres A, Bekar LK, Takano T, et al. Critical role of aquaporin-4 (AQP4) in astrocytic Ca2+ signaling events elicited by cerebral edema. Proc Natl Acad Sci U S A. 2011; 108 (2) 846–851. DOI: 10.1073/pnas.1015217108 [PubMed: 21187412]

[40]. Norenberg MD, Rao KV, Jayakumar AR. Mechanisms of ammonia-induced astrocyte swelling. Metab Brain Dis. 2005; 20 (4) 303–318. DOI: 10.1007/s11011-005-7911-7 [PubMed: 16382341]

[41]. Ezan P, Andre P, Cisternino S, Saubamea B, Boulay AC, Doutremer S, et al. Deletion of astroglial connexins weakens the blood-brain barrier. J Cereb Blood Flow Metab. 2012; 32 (8) 1457–1467. DOI: 10.1038/jcbfm.2012.45 [PubMed: 22472609]

[42]. Rose CR, Ransom BR. Gap junctions equalize intracellular Na+ concentration in astrocytes. Glia. 1997; 20 (4) 299–307. [PubMed: 9262234]

[43]. Ishimaru S, Okada Y, Mies G, Hossmann KA. Relationship between blood flow and blood-brain barrier permeability of sodium and albumin in focal ischaemia of rats: a triple tracer autoradiographic study. Acta Neurochir. 1993; 120 (1-2) 72–80. [PubMed: 8434521]

Highlight

- Accumulation of noxious metabolites in the interstitial fluid of brain may contribute to hepatic encephalopathy.

- Accumulation of such products may be due to reduced glymphatic clearance mechanisms in the brain.

- We identified regions of impaired glymphatic clearance function, which aligned closely with cognitive/behavioural deficits.

- Reduced AQP4 expression was observed in the same regions.

- Altered AQP4 mediated glymphatic dysfunction may contribute to pathogenesis of hepatic encephalopathy.

Lay summary

The 'glymphatic system' is a newly discovered brain-wide pathway that facilitates clearance of various substances that accumulate in the brain due to its activity. This study evaluated whether the function of this system is altered in a model of brain dysfunction that occurs in cirrhosis. For the first time, we identified that the clearance of substances from the brain in cirrhosis is reduced because this clearance system is defective. This study proposes a new mechanism of brain dysfunction in patients with cirrhosis and provides new targets for therapy.
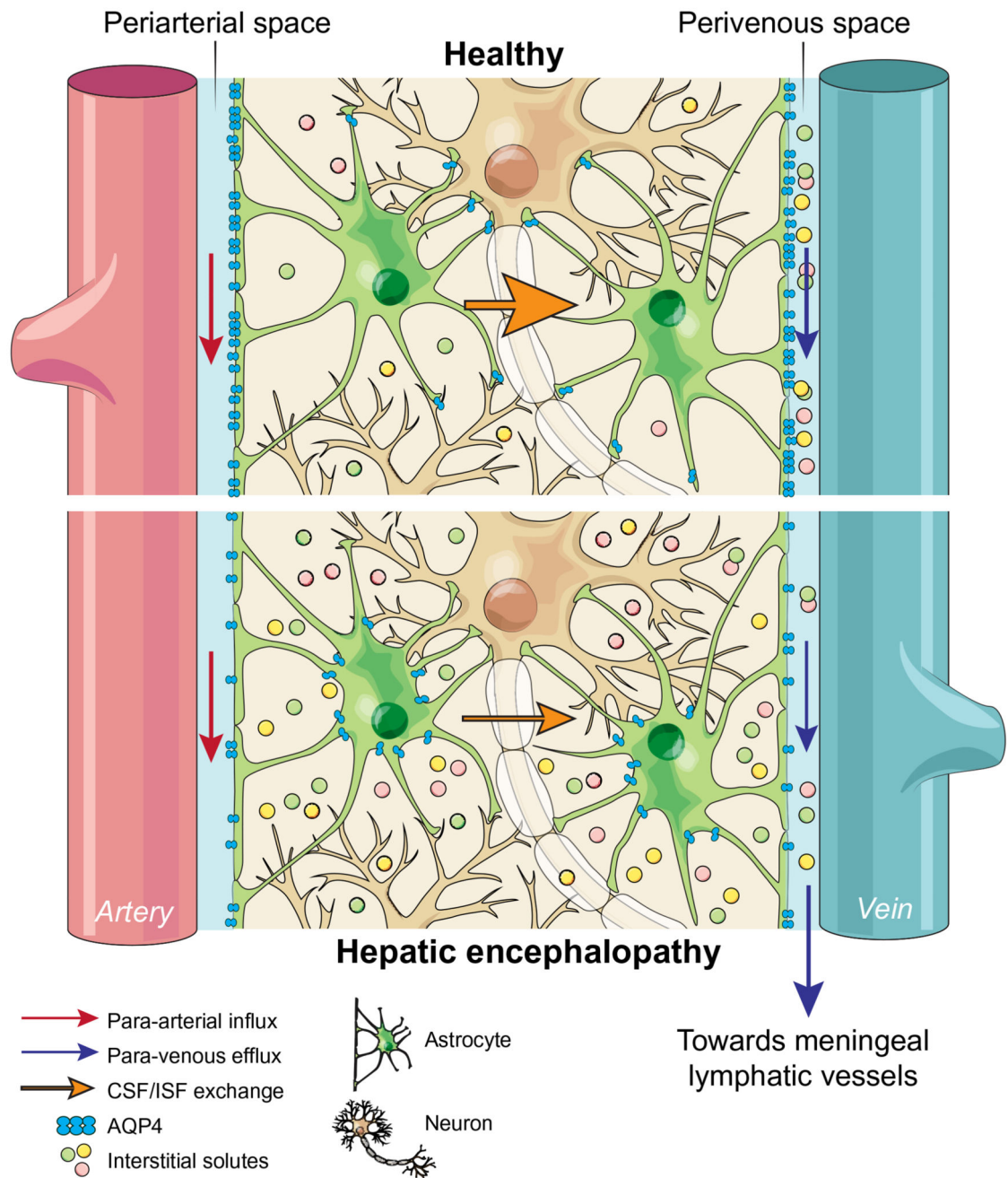
Fig. 1. Schematic of proposed alterations in glymphatic function in hepatic encephalopathy.
In health, glymphatic inflow of CSF occurs parallel to arterial flow along the periarterial space (between the basement membrane of smooth muscle cells and pia mater), where the water component of CSF crosses the astrocytic AQP4 channels polarised to astrocyte end-feet and enters the brain parenchyma. Here, CSF exchanges with ISF, allowing interstitial solutes to be cleared out of the parenchyma via astroglial transporters or channels, or pass through the astrocytic end-feet clefts to the perivenous space. Effluxed waste is then cleared out of the CSF pool via absorption by the meningeal lymphatic system. In

hepatic encephalopathy, our data suggests that this brain-wide clearance system becomes dysfunctional, possibly because of reduced vessel coverage and polarisation of AQP4, leading to toxic accumulation of interstitial solutes in the parenchyma. Arrows indicate direction of flow. AQP4, aquaporin-4; CSF, cerebrospinal fluid; ISF, interstitial fluid.
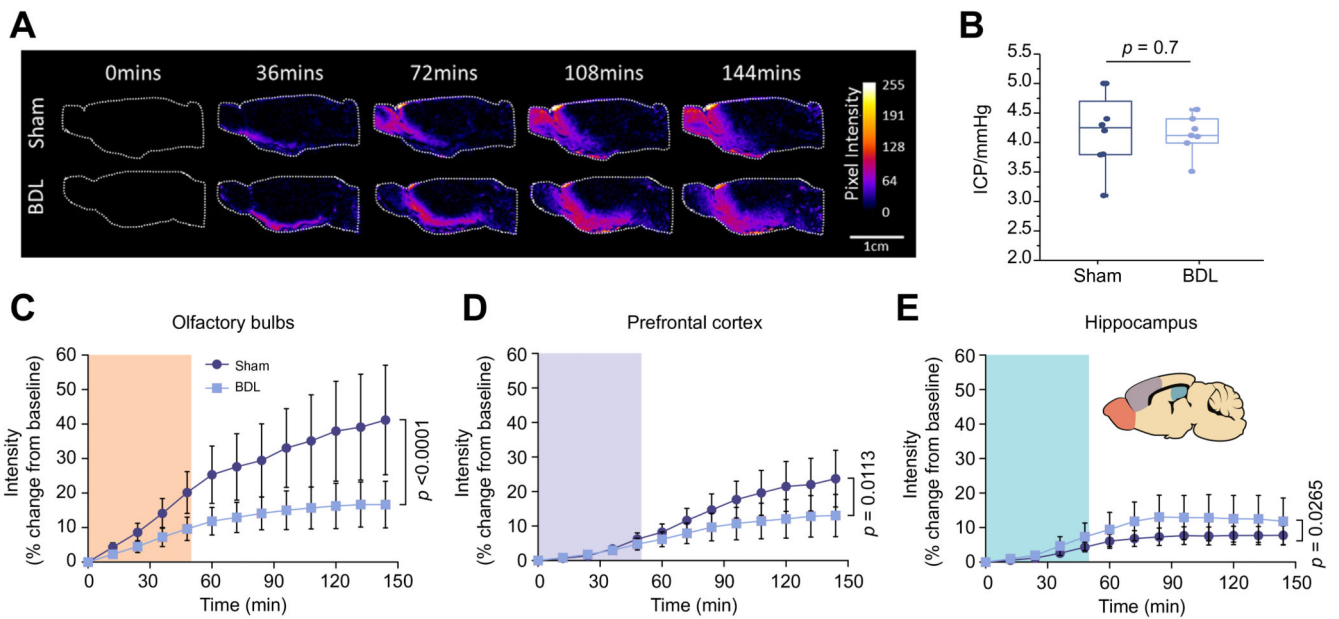
Fig. 2. Impaired contrast agent penetration in the brain of animals with HE.
(A) Representative images of dynamic contrast-enhanced MRI of sham-operated (n = 5) and BDL (n = 5) animals. Pseudocolour scaling illustrates distribution of gadolinium throughout the brain over 144 min of recording, with the BDL brain showing reduced contrast agent and therefore glymphatic inflow in rostral areas. (B) Summary data illustrating resting ICP in sham-operated and BDL animals. Summary data showing MR contrast intensity changes in the (C) olfactory bulb (D) prefrontal cortex and, (E) hippocampus of sham-operated and BDL rats. Inset: Schematic drawing illustrating brain regions of interest. Shading indicates period of contrast agent infusion. Statistical comparisons were performed using 2-way ANOVA followed by Bonferroni post hoc test. p values indicate the level of significant differences between the groups. BDL, bile duct ligation; HE, hepatic encephalopathy.
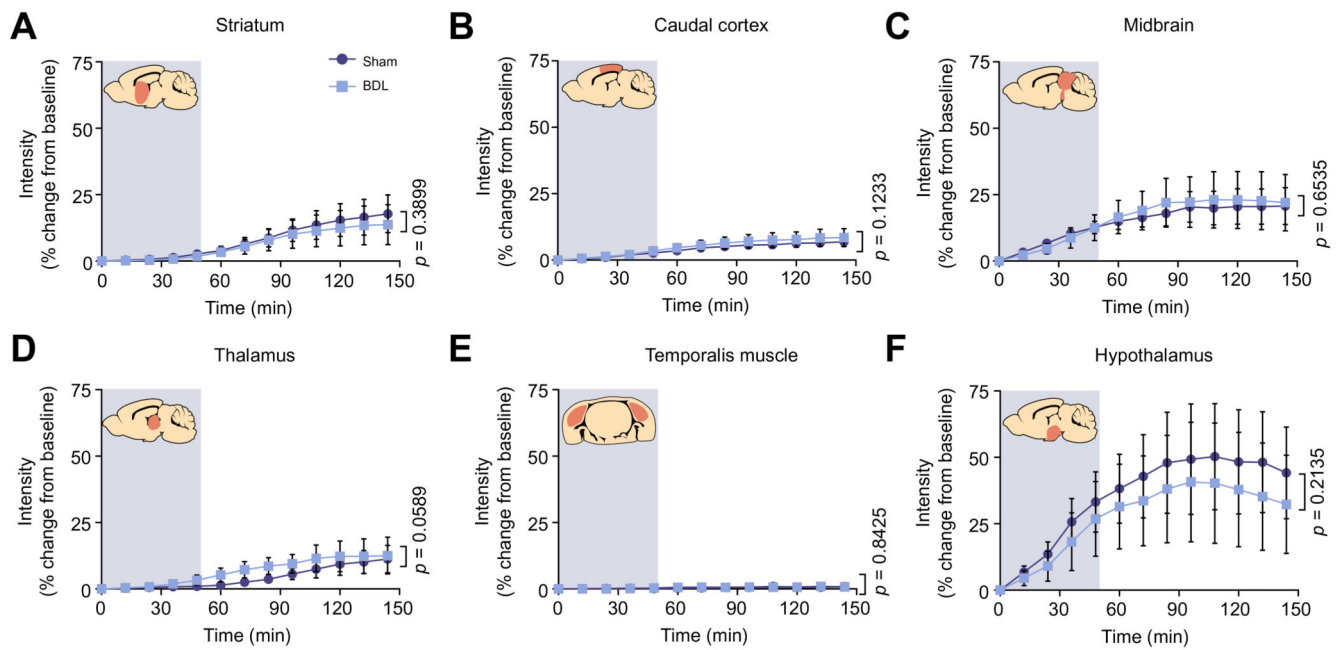
Fig. 3. Unchanged contrast agent penetration in the striatum, caudal cortex, midbrain, thalamus, and hypothalamus of animals with HE.

Intensity (% change from baseline) *vs.* time plots of contrast agent penetration showing no difference between sham-operated (n = 5) and BDL (n = 5) rats in the (A) striatum, (B) caudal cortex, (C) midbrain, (D) thalamus, (E) temporalis muscle, acting as negative control with lack of contrast agent in the temporalis muscle representing a sealed system and no CSF leakage due to the cannula implantation, and (F) hypothalamus. Grey shading indicates period of contrast agent infusion. Statistical comparisons were performed using 2-way ANOVA followed by Bonferroni *post hoc* test. *p* values indicate the level of differences between the sham-operated and BDL groups. BDL, bile duct ligation; HE, hepatic encephalopathy.
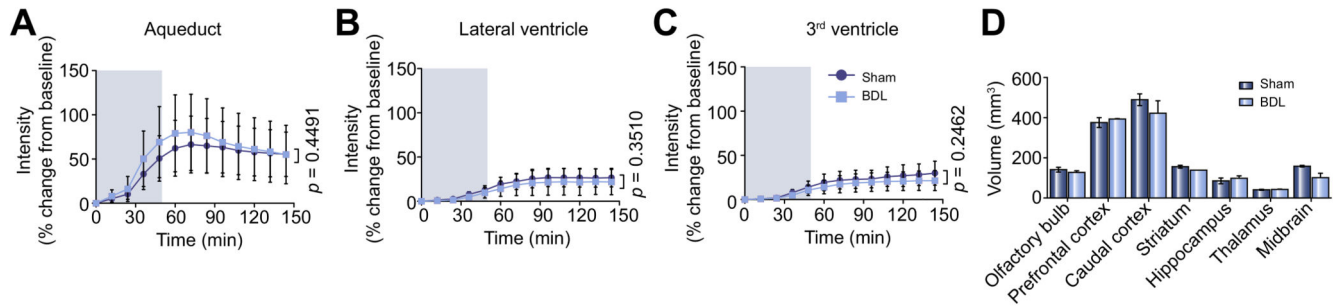
Fig. 4. Contrast agent inflow in CSF filled compartments (aqueduct, lateral ventricles and third ventricle) and volumes of select brain regions are not altered in HE.

Intensity (% change from baseline) *vs.* time plots of contrast agent penetration indicating no difference between sham-operated (n = 5) and BDL (n = 5) rats in the (A) aqueduct, (B) lateral ventricles and (C) 3rd ventricle. Grey shading indicates period of contrast agent infusion. (D) Summary data illustrating volume (mm^3) of the brain regions of interest obtained from 3D ROI measurements of contrast-enhanced MR images from sham-operated and BDL animals, with no significant differences reported. Statistical comparisons were performed using 2-way ANOVA followed by Bonferroni *post hoc* test. *p* values indicate the level of differences between the sham-operated and BDL groups. BDL, bile duct ligation; CSF, cerebrospinal fluid; HE, hepatic encephalopathy; ROI, region of interest.
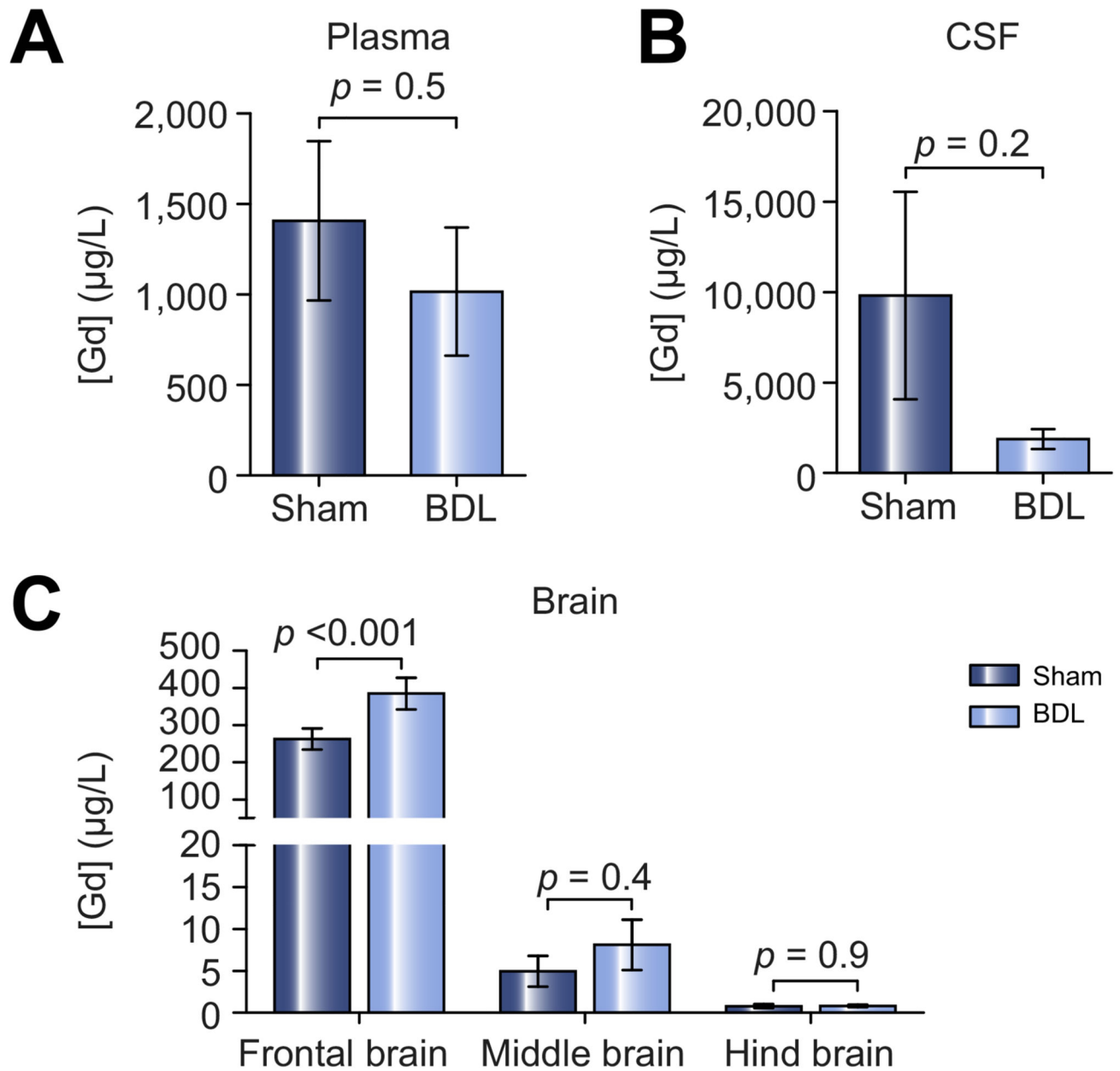
Fig. 5. Impaired Gd-DTPA clearance in the prefrontal cortex, evaluated by SF-ICP-MS in plasma, CSF and brain tissue of animals with HE.

Summary data illustrating Gd concentration in the (A) plasma, (B) CSF and (C) frontal, middle and hind brain tissue of sham-operated (n = 6) and BDL (n = 6) animals. Statistical comparisons for CSF and plasma samples were performed using a Student's *t* test while statistical comparisons of brain data were performed using 2-way ANOVA followed by Bonferroni *post hoc* test. *p* values indicate the level of differences between the sham-operated and BDL groups. BDL, bile duct ligation; CSF, cerebrospinal fluid; HE, hepatic encephalopathy.
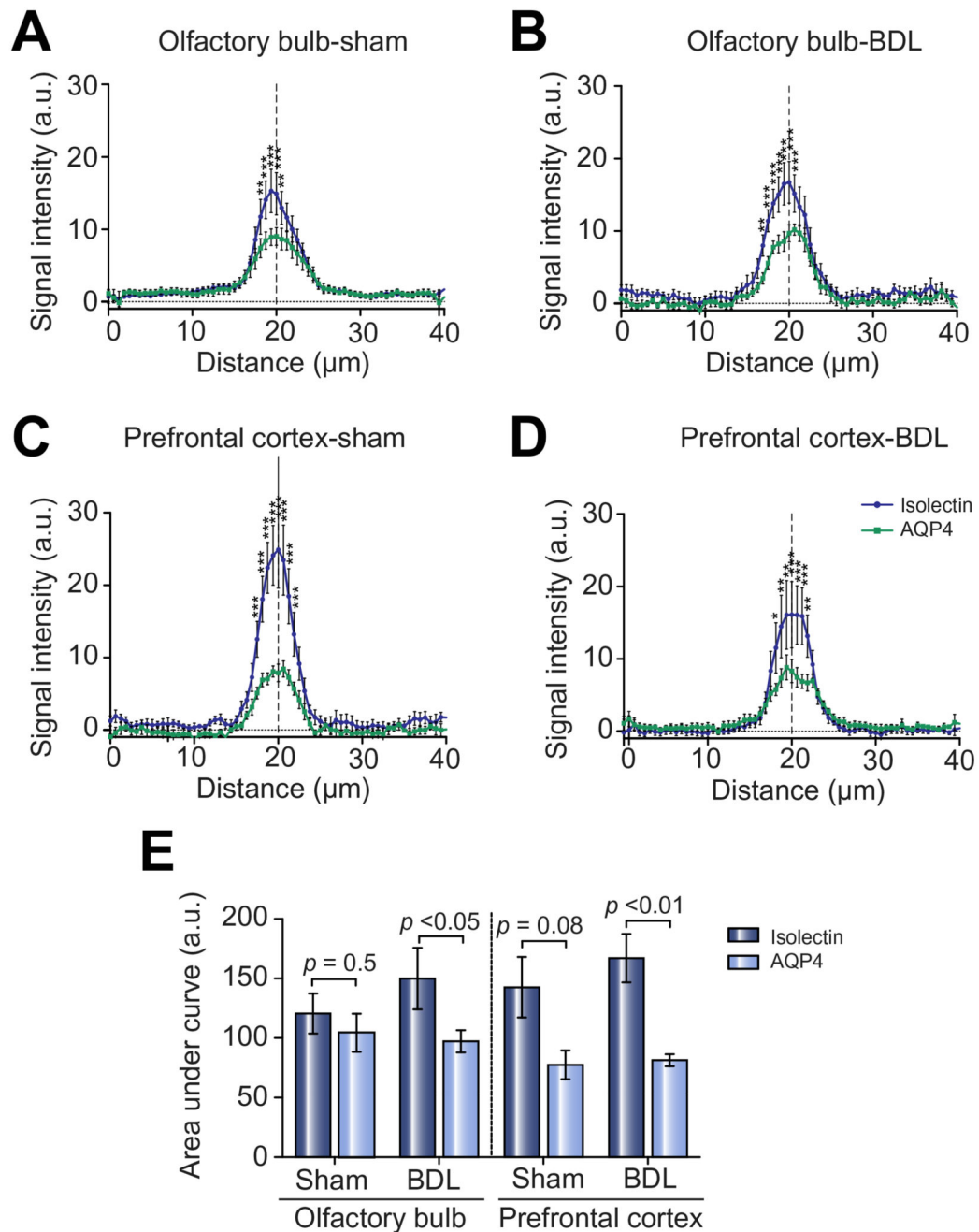
Fig. 6. Altered AQP4 *vs*. Isolectin expression, in the olfactory bulb and prefrontal cortex of animals with HE.

(A-D) Plots of fluorescence signal intensity *vs.* distance across blood vessels for AQP4 and Isolectin expression in the olfactory bulb and prefrontal cortex of sham-operated (n = 4) and BDL rats (n = 4). (E) Summary data indicating area under the curve of the peaks in the intensity graphs, showing significantly lower AQP4 expression compared to Isolectin in both the olfactory bulb and prefrontal cortex of BDL compared to sham-operated animals. Statistical comparisons between immunofluorescence line profile data, and area under the curve were performed using 2-way ANOVA followed by Bonferroni *post hoc* test. For

within group comparison *p <0.05, **p <0.01, ***p <0.001. *p* values indicate the level of differences between Isolectin and AQP4 within each animal group. AQP4, aquaporin-4; BDL, bile duct ligation.
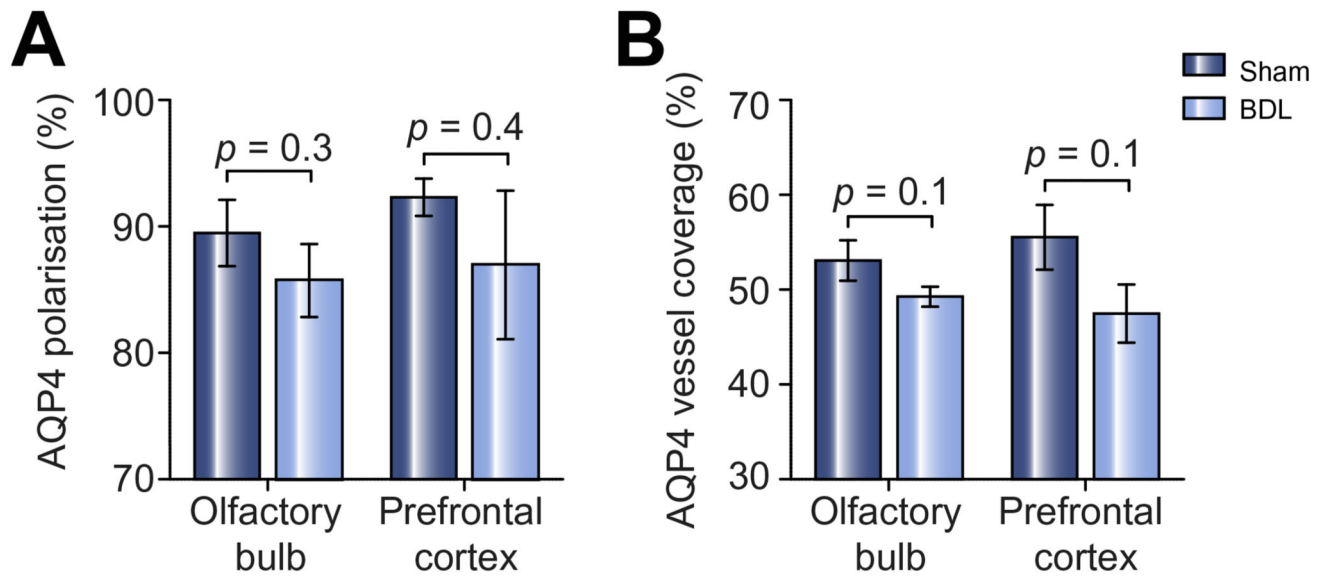
Fig. 7. AQP4 polarisation and vessel coverage is not significantly lower in the olfactory bulb and prefrontal cortex of animals with HE.
(A) Summary data illustrating AQP4 polarisation in the olfactory bulb and prefrontal cortex of sham-operated and BDL animals, with no significant differences reported. (B) Summary data illustrating AQP4 vessel coverage in the olfactory bulb and prefrontal cortex of sham-operated and BDL animals, with no significant differences reported. Statistical comparison was performed using 2-way ANOVA followed by Bonferroni *post hoc* test. *p* values indicate the level of differences between the sham-operated and BDL groups. AQP4, aquaporin-4; BDL, bile duct ligation; HE, hepatic encephalopathy.
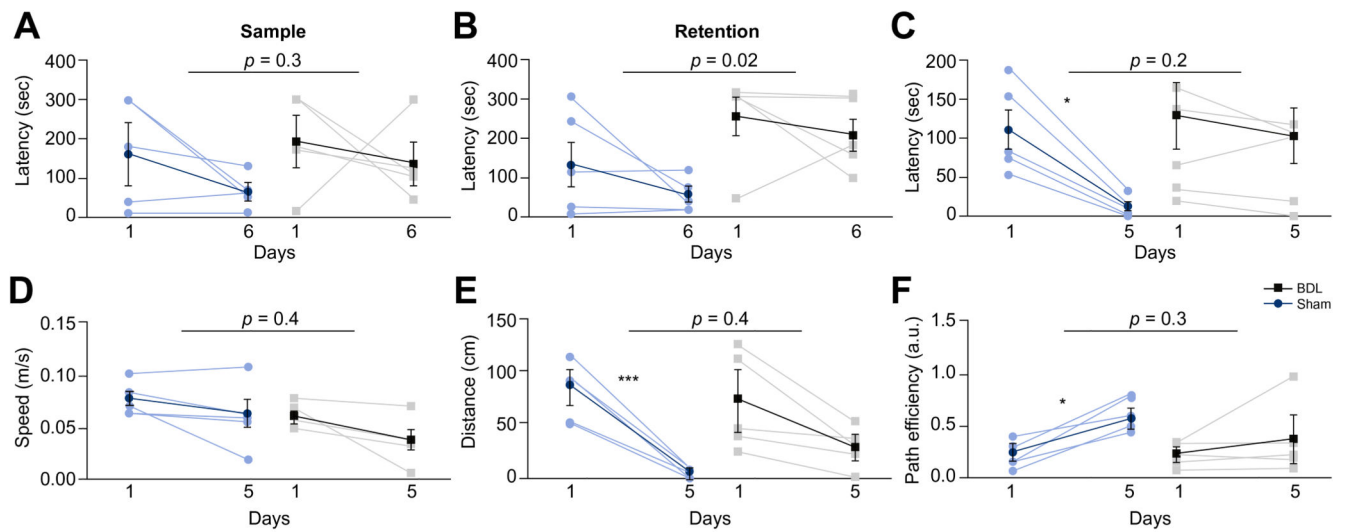
Fig. 8. Cognitive/behavioural deficits in HE.

(A) Summary data illustrating time latency required to reach the escape box in the working memory task in sham-operated (n = 5) and BDL (n = 5) rats. Summary data illustrating (B) retention latency in the working memory task, (C) latency, in the spatial reference memory task, (D) speed of animal during the reference memory task, (E) distance travelled during the reference memory task and (F) path efficiency from the starting point to the escape box during the reference memory task comparing sham-operated and BDL rats. Statistical comparisons of data between sham-operated and BDL animals were performed via 2-way ANOVA with Bonferroni post hoc test. For comparison of data within animal groups along training days, 2-way ANOVA was applied followed by Tukey *post hoc* test. *p* values indicate the level of significant differences between the sham-operated and BDL groups. For within group comparison *p <0.05, ***p <0.001. BDL, bile duct ligation.